Humanized substitutions of *Vmat1* in mice alter amygdala-dependent behaviors associated with the evolution of anxiety

Daiki X. Sato[1, #†], Yukiko U. Inoue[2†], Yuki Morimoto[2], Takayoshi Inoue[2], Nahoko Kuga[3], Takuya Sasaki[3, 4], Yuji Ikegaya[3, 5, 6], Kensaku Nomoto[7], Takefumi Kikusui[8], Satoko Hattori[9], Giovanni Sala[9], Hideo Hagihara[9], Tsuyoshi Miyakawa[9] and Masakado Kawata[1]*

[1]Graduate School of Life Sciences, Tohoku University, Sendai, Miyagi 980-8578, Japan
[2]Department of Biochemistry and Cellular Biology, National Institute of Neuroscience, National Center of Neurology and Psychiatry, Kodaira, Tokyo 187-8502, Japan
[3]Graduate School of Pharmaceutical Sciences, The University of Tokyo, 7-3-1 Hongo, Bunkyo-Ku, Tokyo 113-0033, Japan
[4]Precursory Research for Embryonic Science and Technology (PRESTO), Japan Science and Technology Agency (JST), 4-1-8 Honcho, Kawaguchi, Saitama 332-0012, Japan
[5]Center for Information and Neural Networks, National Institute of Information and Communications Technology, 1-4 Yamadaoka, Suita City, Osaka, 565-0871, Japan
[6]Institute for AI and Beyond, The University of Tokyo, Tokyo 113-0033, Japan
[7]Department of Physiology, Dokkyo Medical University, Mibu, Tochigi, 321-0293, Japan
[8]Department of Animal Science and Biotechnology, Azabu University, Kanagawa, Japan
[9]Division of Systems Medical Science, Institute for Comprehensive Medical Science, Fujita Health University, Toyoake, Aichi 470-1192, Japan
[#]Present address: Graduate School of Science, Chiba University, Chiba, 263-8522, Japan

[†]equally contributed
*corresponding author: kawata@tohoku.ac.jp, TEL +81-22-795-6688

Keywords
Vmat1, anxiety, amygdala, human evolution, CRISPR/Cas9

Abstract

The human vesicular monoamine transporter 1 (*VMAT1*) harbors unique substitutions (Asn136Thr/Ile) that affect monoamine uptake into synaptic vesicles. These substitutions are absent in all known mammals, suggesting their contributions to distinct aspects of human behavior modulated by monoaminergic transmission, such as emotion and cognition. To directly test the impact of these human-specific mutations, we introduced the humanized residues into mouse *Vmat1* via CRISPR/Cas9-mediated genome editing and examined changes at the behavioral, neurophysiological and molecular levels. Behavioral tests revealed reduced anxiety-related traits of *Vmat1*^{Ile} mice, consistent with human studies, and electrophysiological recordings showed altered oscillatory activity in the amygdala under anxiogenic conditions. Transcriptome analyses further identified amygdala-specific changes in the expression of genes involved in neurodevelopment and emotional regulation, which may corroborate the observed phenotypes. This knock-in mouse model hence provides compelling evidence that the mutations affecting monoaminergic signaling and amygdala circuits have contributed to the evolution of human socio-emotional behaviors.

Introduction

Recent years have seen a surge in the study revealing distinct human brain characteristics at the molecular, cellular, and circuit levels in both cortex and subcortical structures (1–4). Differences in brain monoaminergic signaling are likely to be key factors conferring human attributes, as various monoaminergic pathways are involved in emotional regulation, memory consolidation, cognitive flexibility, and complex social behaviors (5–7). Comparative studies have indeed demonstrated the distinct monoaminergic mechanisms in the human brain (2, 8). Moreover, diversification of monoaminergic mechanisms has been linked to the evolution of social behavior in non-human primates (9, 10). Thus, genetic differentiation of monoaminergic genes may underlie our unique emotional and social characteristics, such as empathy and altruism (2).

In line with these studies, we recently reported that the vesicular monoamine transporter 1 (*VMAT1*; also known as *SLC18A1*) gene has been under positive selection in the human lineage as evidenced by two amino acid substitutions (Glu130Gly and Asn136Thr) not shared by other primates (11). The VMATs transport monoamine neurotransmitters into synaptic vesicles, thereby regulating the kinetics of synaptic transmission. There are two isoforms of VMAT, VMAT1 and 2, with the VMAT2 being highly expressed in the brain and widely studied (12, 13). In contrast, VMAT1 was previously thought to be expressed solely in the peripheral nervous system and chromaffin cells, and its functional importance in the CNS has only recently been implicated (14). Our previous study showed that a new mutation at the 136th amino

acid (136Ile) of *VMAT1* has emerged relatively recently in the course of human evolution, and that the human-specific polymorphism Thr136Ile has likely been maintained by balancing selection within non-African populations (11). Fluorometric assays additionally demonstrated that these human-specific residues enhance monoamine neurotransmitter uptake, suggesting the tendency of lower monoamine uptake in early hominids (15). The 136Thr, the dominant variant across populations, is known to be marginally associated with psychiatric diseases, such as bipolar disorder, depression and anxiety, as well as with the neuroticism, a personality trait conferring greater risk of psychiatric disease (16–18). Thus, higher levels of depression and/or anxiety-like behaviors with 136Thr may have been favored in our ancestors, while more recent selection may have led to the emergence of 136Ile after the migration out of Africa and into harsher environments.

Although the evolution of *VMAT1* and its basic functions in the mammalian CNS have been clarified, their contributions to unique human attributes are still unclear. Here we examine the molecular, neurological, and behavioral changes in mice caused by human-specific *VMAT1* mutations. We show that humanized *Vmat1* (*Vmat1*^{Ile}) induces amygdala-specific changes in gene expression and neuronal activity, reduces anxiety-like behaviors under anxiogenic conditions and even enhances preference for social novelty. These findings suggest that altered monoaminergic signaling in the amygdala has contributed to the evolution of human emotional and social behaviors, and the present work provides a new experimental strategy for evolutionary studies of human emotions.

Results

Conservation of the 136th residue of VMAT1 across non-human vertebrates

To investigate the evolutionary significance of the 136th residue in human VMAT1 (hVMAT1), we first examined the conservation of this residue in a wide range of taxa in vertebrates. Multiple sequence alignments of VMAT1 among 236 vertebrate species revealed the unique evolution of this residue in the human lineage (Fig. 1a). Notably, we confirmed that all species but bicolor damselfish retain asparagine (Asn) at the 136th amino acid, while *Homo sapiens* is the only vertebrate species that carries the unique Thr136Ile (rs1390938) polymorphism.

Predicted effects of humanized residues on mouse VMAT1 structure and function

In silico predictions of wild type mouse VMAT1 (mVMAT1) protein structure revealed that like the hVMAT1 residue 136, the corresponding residue in mVMAT1 (133Asn) was located between the first luminal loop and the second transmembrane domain (Fig. 1b), suggesting a similar function. Given the evolutionary conservation across vertebrates and the difference in chemical properties between amino acids, the humanized mutations to mVMAT1, especially 133Asn to 133Ile, were predicted to have a significant impact on protein function (Table 1). Furthermore, the Asn133Ile mutation was also predicted to stabilize the protein structure as evidenced by greater folding free energy ($\Delta\Delta G$: 1.106 kcal/mol; Table 1) and to increase the flexibility of the loop domain (Fig. 1b), which possibly increases the efficiency of monoamine uptake.

116

117 **Generation of *Vmat1*-humanized mouse models by CRISPR/Cas9 genome editing**

118 In order to replace the 133Asn of mouse Vmat1 with Thr or Ile, we employed the
119 CRISPR/Cas9-mediated genome editing strategy (Fig. 2a). We selected a guide RNA
120 targeting the 133rd Asn codon in *Vmat1* exon 4 by using the web-based CRISPR design
121 tool to minimize off-target cleavage risk (Supplementary Table S1 and 2, see Methods
122 for details). By electroporating CRISPR components (*Vmat1* exon 4 crRNA, tracrRNA,
123 and Cas9 nuclease) along with the ssDNA donor containing the desired substitutions
124 into C57BL/6J fertilized eggs (Fig 2a, Supplementary Fig S1a), we successfully
125 generated 133Thr founder No.1 and 133Ile founder No.10 (Supplementary Fig. S1b, c
126 and d). After confirming the absence of off-target cleavages (Supplementary Fig. S2),
127 we crossed 133Thr founder No.1 and 133Ile founder No.10 with wild type (WT)
128 C57BL/6J mice to obtain heterozygous F1 generations, which were again verified to
129 possess the designed substitutions by Sanger sequencing. The homozygous mice were
130 further crossed after the F5 generations to obtain three humanized genotypes, Thr/Thr,
131 Thr/Ile, and Ile/Ile, in addition to WT, for behavioral, neurophysiological, and
132 transcriptomic analyses (Supplementary Fig. S3, see Methods).

133

134 **The human Ile substitution in mVMAT1 reduced behavioral anxiety**

135 We accordingly conducted comprehensive behavioral tests among the 20 sets of mice
136 including one of each genotype (*Vmat1*^{WT}, *Vmat1*$^{Thr/Thr}$, *Vmat1*$^{Thr/Ile}$, and *Vmat1*$^{Ile/Ile}$)
137 from the 1st batch at 9–55 weeks (see Supplementary Table S3 for detailed information

on age and the number of individuals used in each test). Detailed results were shown in Fig. S4–19. Tests of social interaction (SI) between stranger mice of the same genotype in a novel environment (one-chamber SI test) and of preference for a novel stranger over a previously exposed stranger (now familiar) in Crawley's 3-chamber social interaction (CSI) test revealed marginal differences in behavioral phenotypes between mice with and without *Vmat1*^{Ile} ($P = 0.062$ for interactive effects of genotype (Ile) and place, generalized additive model (GAM) with quasi-Poisson distribution; Fig. 3a, Supplementary Fig. S9 and 10). In the CSI, *Vmat1*$^{Thr/Thr}$ mice significantly preferred familiar to stranger mice ($P = 3.26\times10^{-4}$), while no such tendency was observed in *Vmat1*^{Ile} mice ($P = 0.759$ for *Vmat1*$^{Thr/Ile}$ mice and ($P = 0.195$ for *Vmat1*$^{Ile/Ile}$ mice; Fig. 3a). Moreover, we found consistently lower levels of anxiety among *Vmat1*^{Ile} mice across tests, including relatively greater preference for the (anxiogenic) light box during the two-chamber light/dark transition (LD) test and for the center of an open field (OF) (Supplementary Fig. S5 and 6).

To confirm a pervasive effect on specific behavioral domains by humanized VMAT1, we constructed composite behavioral phenotype scores by summating standardized scores on related tests (LD, OF, elevated plus maze (EP), and SI tests) and compared the results among genotypes. We further conducted Structural Equation Modeling (SEM) to investigate the effects of genotype on these composite scores. This analysis revealed a significant effect of 133Ile on anxiety scores ($R^2 = 0.15$, $P = 8.7\times10^{-3}$) but only marginal effects on locomotor activity ($R^2 = 0.062$, $P = 0.053$; Fig. 3b).

159 Anxiety levels were generally lower in *Vmat1*^{Ile} mice (P = 0.016, one-way ANOVA;
160 Fig 3c).

161 In addition to standard tests of anxiety, exploratory tendency, and locomotor
162 activity, we also performed a novel delayed reward task to evaluate the differences in
163 impulsivity between *Vmat1*$^{Thr/Thr}$ and *Vmat1*$^{Ile/Ile}$ mice (n = 10 for both genotypes, see
164 Methods for detailed experimental procedure; Supplementary Fig. S19a–c). Throughout
165 the test, there was no statistically significant difference in food preference between
166 genotypes (P = 0.50 for the first term, GAM with quasi-Poisson distribution;
167 Supplementary Fig. S19d). However, *Vmat1*$^{Ile/Ile}$ showed a lower preference for the
168 higher-calorie but delayed food reward than *Vmat1*$^{Thr/Thr}$ mice every test day from 5 to 9
169 except for day 6 compared to the basal level after habituation (day 4) (Supplementary
170 Fig. S19d).

171

172 **Differential regulation of dopaminergic and neurodevelopmental genes in the**
173 **amygdala by *Vmat1* genotype**

174 We then conducted RNA-Seq analysis to investigate the effects of the four *Vmat1*
175 genotypes on gene expression patterns in three brain regions likely associated with the
176 behavioral phenotypes (prefrontal cortex, amygdala, and striatum) (n = 4 mice for each
177 genotype; see Supplementary Table S4 for detailed information on samples and reads).
178 Principal component analysis revealed distinct expression patterns among brain areas,
179 but no obvious differences between genotypes and ages (4 vs. 10 months)
180 (Supplementary Fig. S20).

We thus screened for differentially expressed genes (DEGs) by pair-wise comparisons between genotypes, which yielded a total of 80 DEGs exclusively in the amygdala (Fig. 4a). A large proportion of these genes (56 out of 80) were differentially expressed between *Vmat1*^{WT} and *Vmat1*$^{Ile/Ile}$ mice (Fig. 4a). The expression levels of DEGs for each sample were shown in Supplementary Fig. S21. We then utilized the correlations between individual composite anxiety scores and expression levels of the detected amygdalar DEGs among a subset of 8 mice (n = 2 for each genotype). Particularly strong correlations were found for nine genes, *Baz1a*, *Camk2n1*, *Ccdc114*, *Cldn1*, *Fsbp*, *Gdnf*, *Gm42608*, *Gsg1l*, and *KI* ($P < 0.1$; Fig. 4b, Supplementary Fig. S22). The DEGs were further examined for gene ontology (GO) enrichment, which revealed significant overrepresentation of genes involved in "behavior", "fear response", "response to amphetamine", "cardiac muscle tissue development", or "cAMP catabolic process" (Table 2) between WT and Ile/Ile mice, while no GO terms were enriched in DEGs for other genotype comparisons (as there were few such genes). Moreover, gene expression patterns in the Ile mice amygdala were significantly positively correlated with those of striata of transgenic mouse models of Huntington disease ($P < 1.0 \times 10^{-28}$; Supplementary Table S5, Fig. S23).

To further characterize the biological pathways affected by *Vmat1* genotype, we performed weighted gene correlation network analysis (WGCNA; Fig. 4c). A co-expressing gene module (M1; Fig. 4c) stood out as it was significantly overrepresented with DEGs detected in the WT vs. Ile/Ile comparison (odds ratio = 3.79, $P = 2.88 \times 10^{-8}$ by Fisher's exact test) and was negatively correlated with composite anxiety score.

These genes include many involved in adrenergic (*Adra2b*), dopaminergic (*Adcy5*, *Adora2a*, *Drd1*, *Drd2*, *Gnal*, *Gng7*, *Gpr6*, *Gpr88*, *Pde1b*, *Pde1c*, *Pde7b*, *Pde10a*, *Pdyn*, *Penk*, *Ppp1r1b*, *Rasgrp2*, *Rgs9* and *Tac1*), glutamatergic (*Grm4*), and serotonergic (*Htr1b*, *Htr1d*, *Htr1f*, and *Htr4*) signaling pathways. Sub-network analysis further detected another functional gene cluster involved in neural development within the co-expressing module (cluster 2 in Fig. 4d). Strikingly, three genes, *Foxp1*, *Foxp2*, or *Six3*, all of which are important regulators of neural growth, were located in hubs connecting genes involved in postsynaptic signaling (cluster 1) as mentioned above and neural development (cluster 2; e.g., *Dlx6*, *Ebf1*, *Isl1*, and Wnt2).

The humanized mVMAT1 disrupted anxiety-associated theta band activity in the basolateral amygdala

Aforementioned behavioral and transcriptomic results suggest that the *Vmat1* genotype influences anxiety-related neuronal activity patterns. Inspired by a previous report that theta (4–12 Hz) oscillations in the medial prefrontal cortex (mPFC) and basolateral amygdala (BLA) are specifically enhanced under anxiogenic environments such as the open arms of an elevated plus maze (EP) and the center area of an OF (19, 20), we next performed simultaneous local field potential (LFP) recordings from the dorsomedial prefrontal cortex (dmPFC) and BLA in freely moving mice during elevated plus maze (EP) exploration (Fig. 5a; n = 11 dmPFC and 9 BLA electrodes from 5 $Vmat1^{WT}$, n = 6 and 6 electrodes from 4 $Vmat1^{Thr/Thr}$ and n = 10 and 7 electrodes from 4 $Vmat1^{Ile/Ile}$ mice). The histological confirmation of electrode positions and raw LFP signals were

shown in Fig. 5b and c, respectively. Power spectral analysis of WT mice revealed lower 4–7 Hz power in both dmPFC and BLA during exploration of the EP open arms compared to close arms, suggesting a relationship with anxiety-like behavior (Fig. 5d). Further, the Granger causality test revealed the directionality of 4–7 Hz oscillations from the mPFC to BLA (Fig. 5e; n = 20 electrode pairs from 5 *Vmat1*^{WT} mice), consistent with anatomical evidence that the dmPFC preferentially projects to the BLA (21, 22) and that mPFC theta oscillations drive BLA neuronal activity (20). Based on these observations, we compared 4–7 Hz power in dmPFC and BLA among genotypes. Both WT and *Vmat1*$^{Thr/Thr}$ mice exhibited significantly lower LFP 4–7 Hz signal power in dmPFC and BLA under the anxiogenic condition of open arm exploration compared to closed arm exploration, while *Vmat1*$^{Ile/Ile}$ mice showed no such consistent activity pattern in the BLA (Fig. 5f), suggesting that anxiety-related neuronal mechanisms in the dmPFC–BLA circuit are disrupted by the *Vmat1*$^{Ile/Ile}$ genotype.

Discussion

While the potential importance of *VMAT1* in neuroendocrine signaling has been suggested, few studies have focused on this gene until recently, largely due to its low expression in the central nervous system (12, 23, 24). A series of studies, however, have demonstrated the psychopathological effects of this gene and suggests its importance in emotional regulation. The Thr136Ile polymorphism (rs1390938) is allegedly associated with bipolar disorder (16), autism spectrum disorder (25), cognitive function related to schizophrenia (26), anxiety, depressiveness, neuroticism, or maladaptive impulsivity

(18). Our previous study uncovered from an evolutionary perspective that this variant is a human-specific polymorphism (as shown in Fig. 1a) and under positive selection in the human lineage (11). Two substitutions (i.e., Glu130Gly and Asn136Thr) occurred in the human lineage after the divergence from the common ancestor of chimpanzees and humans, and these substitutions combined have been shown to decrease the monoamine uptake of VMAT1 (15). On the other hand, the new "hyper-function" allele (i.e. 136Ile; Lohoff et al. 2014), which increases the monoamine uptake of VMAT1 and is associated with fewer psychopathological symptoms by contrast, emerged just before the Out-of-Africa event of modern humans and is currently 20–61% in frequency in non-African populations (11). We also found that the Thr136Ile polymorphism has been under balancing selection in non-African populations (11). Given such evolutionary significance and psychopathological effects of the Thr136Ile polymorphism in *VMAT1*, this variant could play a very important role in exploring the evolutionary origins of human psychological traits and their diversity.

Phenotypic changes in mice caused by the humanized *Vmat1*

Our comprehensive behavioral tests show the protective effects of the $Vmat1^{Ile}$ allele against anxiety-like behavior (Fig. 3b and c), which is well consistent with the human phenotype (18). Compared to $Vmat1^{Ile}$ ($Vmat1^{Thr/Ile}$ and $Vmat1^{Ile/Ile}$) mice, both wild-type and $Vmat1^{Thr/Thr}$ mice showed similar behavioral phenotypes and have higher levels of anxiety in both solitary (LD, EP, and OF) and social (SI and CSI) environment. This is expected from the molecular evidence that 136Asn and 136Thr are comparable in the

level of monoamine uptake, which is lower than that of 136Ile (15). It is noteworthy that the genotypic effect was not observed for fear response of mice (Supplementary Fig. S16). Given the potential difference in neurological mechanism behind fear and anxiety (27, 28), Vmat1 may specifically regulate anxiety-related circuits of the brain as discussed later. The results of delayed reward task may suggest that the *Vmat1*$^{Ile/Ile}$ mice are more impulsive, at least initially, under this condition but contradicts an epidemiological study reporting an association of 136Thr with maladaptive impulsivity (18). Kim et al. (2018) reported that the deletion of the D2 dopamine receptor (D2R) increased impulsive behavior in mice, whereas restoration of D2R in the amygdala alone normalized impulsive behavior (29). This is compatible with our results, as dopaminergic genes including *Drd2* were downregulated in *Vmat1*$^{Ile/Ile}$ mice (Supplementary Fig. S24). The possible difference in association of *VMAT1* genotype with impulsivity between humans and mice may stem from functional connectivity changes in related neural circuits and warrants further investigation. Overall, these observations suggest that the 136Ile substitution may contribute to uniquely human behavioral traits that have propelled both our technological progress and adaptation to almost all ecosystems, namely high exploratory tendency and relatively lower anxiety under threatening or novel conditions. Indeed, 136Ile allele frequency increases along the migration route of modern humans (11), suggesting that the exploratory tendency and/or boldness conferred by this mutation was advantageous for survival. In this regard, *Vmat1*^{Ile} is analogous to the D4R polymorphism associated with novelty-seeking behavior (30).

Differentially expressed genes were significantly enriched in those downregulated in *Vmat1*$^{Ile/Ile}$ and involved in behavioral control and/or fear response as well Huntington disease (HD). It is possible that the Ile mice recapitulate some dimensions of HD pathology, given that dopamine (DA) signaling likely plays a significant role in HD, and the only current FDA-approved drug for HD is a VMAT2 inhibitor, tetrabenazine (31). WGCNA detected a co-expressing module (M1; Fig. 4c) in which the DEGs were significantly overrepresented and revealed that many genes involved in monoaminergic signaling pathways were co-expressed with the detected DEGs (Fig. 4d). Lohoff et al. reported that *Vmat1* KO affected DA signaling in particular, with upregulation of D2R and downregulation of tyrosine hydroxylase (TH) observed in both the frontal cortex and striatum (32). Given the association between *Vmat1* KO and decreased DA in the frontal cortex, we speculated that *Vmat1*$^{Ile/Ile}$ mice would also exhibit downregulation of D2R and upregulation of TH compared to WT mice. Indeed, D2R (along with many other dopaminergic pathway genes) was downregulated in *Vmat1*$^{Ile/Ile}$ mice compared to WT mice. However, there were no significant differences in TH expression among genotypes (Supplementary Fig. S24), suggesting that the *Vmat1* Ile allele alters dopaminergic transmission but not DA synthesis. The sub-network analysis detected another functional gene cluster involved in neural development within the co-expressing module (cluster 2 in Fig. 4d), such as *Foxp1*, *Foxp2*, *Six3*, *Dlx6*, *Ebf1*, *Isl1*, and *Wnt2*. Foxp1 (forkhead box protein P1) is a transcription factor that regulates the development of various tissues including the brain. Foxp1 heterodimerizes with Foxp2, and a human-specific Foxp2 substitution is

313 associated with language impairment (33, 34). Foxp2 also regulates D2R expression
314 (35) and extracellular DA levels (34), potentially involved in the neural development
315 (36), while the cluster 2 genes *Dlx6*, *Ebf1*, *Isl1*, and *Six*3 are all implicated in the
316 development of striatal neurons that express DA receptors (37–39). The DEG Wnt2
317 (also known as Irp) has been found to increase dopaminergic neurons by inducing the
318 proliferation of progenitor cells in the developing midbrain (40). The differential
319 expression of these genes may also be related to the regulatory role of VMAT1 in
320 hippocampal neurogenesis (41), which emerging evidence suggests is associated with
321 anxiety-like behavior (42, 43). Taken together, the differential regulation of DA
322 signaling by *Vmat1* genotypes may have widespread effects on neural development and
323 plasticity.

324 The electrophysiological analysis revealed abnormal neuronal activity in the
325 amygdala of *Vmat1*$^{Ile/Ile}$ mice under fearful conditions (i.e., open arms in EP test; Fig.
326 5f). This was not seen in the medial prefrontal cortex, and thus suggests that amygdala-
327 specific neuronal disturbance underlies the reduced anxiety-like behavior associated
328 with this genotype. This is consistent with a functional imaging study showing that
329 136Ile was associated with increased reactivity and decreased habituation of amygdala
330 toward threat-related stimuli in humans (14). Additional studies are required to reveal
331 the precise association between these LFP changes and amygdalar output in *Vmat1*^{Ile}
332 mice. In light of our behavioral results, we suggest that *Vmat1*^{Ile} may promote the
333 activity of neurons that dampen anxiety, such those projecting from the BLA to the
334 central amygdala (44, 45).

335

336 **Amygdala-specific transcriptomic and neuronal changes associated with anxiety**
337 **imply intra- and inter-species differences in emotion and social behavior**

338 One of the major findings of this study is that *Vmat1* genotype affected transcriptomic
339 regulation and neuronal activity primarily in the amygdala. Given that amygdalar DA
340 signaling is a powerful modulator of fear and anxiety (46), the alterations in gene
341 expression and oscillatory neuronal activity likely contribute to the observed reduction
342 in anxiety-like behaviors among *Vmat1*^{Ile} mice compared to WT mice. The abnormal
343 neuronal activity pattern detected in the amygdala but not PFC of *Vmat1*^{Ile} mice may
344 stem from a difference in VMAT1 expression levels across the brain. Previous studies
345 verified that *VMAT1* mRNA and protein expression levels are relatively high in the
346 amygdala compared to other brain regions in both rats and humans (16, 47). Our
347 transcriptome analysis also revealed higher expression of *Vmat1* in the amygdala than in
348 the striatum (P = 0.0097, Dunnett's test; Supplementary Fig. S25). In contrast, *Vmat2*
349 expression was comparable across regions (Supplementary Fig. S25), indicating
350 distinctive regional regulation between subtypes as shown in a previous study (41).
351 However, the detailed transcriptomic effects of Vmat1 on various types of neurons
352 within the amygdala and possible contributions of peripheral monoamine signaling to
353 them are still unclear, and thus need to be investigated with greater spatial resolution in
354 future studies.

355 Neuronal circuits within the amygdala store associations between
356 environmental cues and adverse stimuli as changes in synaptic strength, and these

357 modified circuits drive the expression of emotion-related behaviors and physiological
358 responses. Thus, the amygdala is a critical regulator of emotional and social behaviors
359 (48), and in fact amygdalar dysfunction is implicated in a number of neuropsychiatric
360 disorders (49–51). Although it is an evolutionarily primitive brain region with relatively
361 well conserved gross structure and general function across species (45), recent studies
362 have provided evidence for more subtle structural and/or functional differences within
363 and among species potentially linked to differential regulation of monoaminergic
364 signaling via VMAT1. The size of the amygdala has been shown to correlate with
365 creativity (52) , mental state inference (53), and the size and complexity of social
366 networks in humans (54) and non-human primates (55). The DA response in the medial
367 amygdala network is associated with mother−infant bonding (56). Collectively, these
368 findings strongly suggest a substantial contribution of the amygdala to evolution of the
369 human social brain by acting as a hub among brain networks associated with emotion,
370 cognition, and communication (57).
371
372 **A single substitution in humanized mouse models highlight molecular and**
373 **neurological evolution underlying human emotional traits**
374 Genetic deletion (KO) and overexpression have become predominant strategies for
375 examining the neurological, behavioral, and pathogenic functions of specific genes.
376 However, gene deletion and overexpression may alter the expression levels of many
377 additional genes, and thus the observed phenotype may be distinct from that induced by
378 target-specific pharmacological manipulations. The present study employed an

379 alternative "knock-in" strategy of a non-synonymous *Vmat1* mutation and succeeded in
380 capturing moderate differences in transcriptomic, neuronal, and behavioral phenotypes.
381 Noticeably, the variant evaluated is a human-specific substitution (i.e., Thr136Ile of
382 *VMAT1*) under selection that is not possessed by other mammals (Fig. 1a). This knock-
383 in model thus provides a unique opportunity to examine the molecular and neurological
384 mechanisms that distinguish human behavior from that of other primates. Such
385 extensive functional analysis of a single mutation has been limited to a few genes such
386 as *FOXP2* (34, 58) and never for effects on emotional traits (59). Therefore, the present
387 study is the first to suggest a new experimental strategy for studies on the evolution of
388 human brain mechanisms underlying emotion and related behavioral traits.
389 Lastly, it needs to be noted that recent genome-wide association studies
390 (GWAS) on psychiatric disorders such as depression (60) and schizophrenia (61), and
391 on specific personality traits (62) have not detected VMAT1 as a top hit despite alleged
392 associations with these phenotypes under study (18, 63). This may indicate that
393 VMAT1 has a weaker influence on phenotype than other significant loci, or that this
394 gene must interact with other loci (epistasis) and/or environmental factors (G × E
395 interaction) for measurable effects on phenotype. Such dependence on other genes or
396 external factors could obscure phenotypic associations of VMAT1 evaluated by
397 conventional approaches of GWAS. In fact, we found that a single amino acid
398 substitution (Asn133Ile) altered the expression of 56 genes within the amygdala, any or
399 all of which may contribute to the observed changes in behavioral phenotype. The
400 effects of various environmental factors (which were largely controlled in this

401 experiment through group housing and shared dams) and DEGs on these behavioral and

402 neurological phenotypes would warrant further study.

Methods

Fully detailed and referenced methods are available in Supplementary Methods.

Phylogenetic analysis and *in silico* prediction of mVMAT1 structure with humanized residues

A phylogenetic tree was constructed from 263 orthologous sequences of vertebrate *SLC18A1* (*VMAT1*), including an archaic hominin sequence that was constructed by replacing 136Ile in the human reference sequence with 136Thr. Homology modeling of the mouse VMAT1 (mVMAT1) protein structure was performed using the SWISS-MODEL (64) web server (http://swissmodel.expasy.org) with the visualization by using PyMOL 2.4.1 (DeLanoScientific, San Carlos, CA). Provean v1.1.3 (65) and SIFT (66) were used to estimate the intolerance for individual amino acid mutations introduced in mVMAT1 based on the evolutionary conservation and the chemical properties of the exchanged residues. DynaMut (67) was also used to evaluate the effects of humanized mutations on the stability and flexibility of VMAT1 protein structure.

Generation of *Vmat1*-humanized mouse models by CRISPR/Cas9 genome editing

See Supplementary Methods for the detailed design and preparation of guide RNA and single-strand DNA (ssDNA) donors targeting mouse *Vmat1*. In addition to the intended humanization, the synonymous substitutions depicted in Fig. 2a were introduced near the 133rd site to prevent unwanted re-editing and enable PCR genotyping. The guide RNAs, Cas9 proteins, and the donor ssDNAs were electroporated into mouse zygotes

425 following the standard protocol (68) to obtain founder knock-in mice (Supplementary
426 Fig S1a). The 133Thr and 133Ile knock-in founders were screened by PCR-RFLP assay
427 (Supplementary Fig. S1c), followed by Sanger sequencing to confirm the correct
428 substitution (Supplementary Fig. S1d). To exclude the possible side effects from off-
429 target cleavages, we sequenced 12 more potential off-target candidate loci predicted by
430 CRISPOR (69) (http://crispor.org) (Supplementary Table S2, Supplementary Fig. S2).
431 After confirming the absence of off-target cleavages, 133Thr founder No.1 and
432 133Ile founder No.10 were crossed with WT C57BL/6J mice to obtain heterozygous F1
433 generations, which were again verified to possess the designed substitutions by Sanger
434 sequencing. For behavioral tests, F5 or F6 homozygous mice were crossed to obtain
435 Thr/Thr, Thr/Ile, and Ile/Ile genotypes. In addition, C57BL/6J WT males and females
436 carrying the Asn/Asn genotype were crossed to supply control mice. To eliminate
437 differences in rearing environment, newborn males of the 4 genotypes (Asn/Asn,
438 Thr/Thr, Thr/Ile, and Ile/Ile) were grouped in sets and nursed by the same mothers.
439
440 **Animal care and experimental conditions for behavioral tests**
441 Animals were housed in groups of four individuals of each genotype under a 12 h
442 light/dark cycle (7:00 AM to 7:00 PM) with ad libitum access to food and water. Adult
443 male mice were used in all tests to eliminate the behavioral effects of the estrus cycle.
444 The composition of cohorts and ages of the mice for every experiment are summarized
445 in Supplementary Table S3. All behavioral tests were conducted in a soundproof room,
446 and as much effort as possible was spent on controlling the effects of confounding

447 factors such as light intensity, temperature, and humidity for the tested group of cage
448 mates. Furthermore, to minimize the impact of one test on subsequent tests in individual
449 mice, behavioral assessments were conducted in the following order after general health
450 and neurological screens: light/dark transition (LD), open field (OF), elevated plus maze
451 (EP), hot plate, social interaction in a novel environment (SI), rotarod, Crawley's 3-
452 chamber social interaction test (CSI), startle response/prepulse inhibition, Porsolt forced
453 swim, T-maze, Barnes maze, tail suspension, fear conditioning, and home cage social
454 interaction tests. See Supplementary Methods for detailed descriptions of behavioral
455 tests.

456 All animal care protocols and experiments were performed according to
457 guidelines approved by the Animal Care and Use Committee of the National Institute of
458 Neuroscience, National Center of Neurology and Psychiatry (approval numbers:
459 2017005, 2020007), the Animal Experiment Committee of Fujita Health University
460 (approval number: APU19063), and the Experimental Animal Ethics Committees of
461 Graduate School of Medicine, and the University of Tokyo (approval number: P29-14).
462

463 **Statistical analyses and Structural Equation Modeling (SEM)**

464 In order to capture overall behavioral patterns among genotypes, we analyzed two major
465 domains of mouse behavior, activity and anxiety, by standardizing, normalizing, and
466 combining sets of related behavioral scores. Total distances traveled in LD, OF, EP, SI,
467 and CSI were used as indices for activity, while time in the light compartment of the LD
468 shuttle box, duration in the central area of the OF, time spent in open arms of the EP,

and total duration of active contacts in the SI were used as indices of anxiety. To confirm the effects of *Vmat1* genotype on the behavioral composites and to enhance statistical power and improve reliability, we used Structural Equation Modeling (SEM) (70). The SEM model included a measurement model and a regression model. The measurement model consisted of two latent factors grouping tests of locomotor activity and anxiety-like behavior. The regression model evaluated the effect of genotype on the two latent factors. Goodness of model fit was evaluated by normed Comparative Fit Index (CFI), Root Mean Square Error of Approximation (RMSEA), and the Standardized Root Mean Square Residual (SRMR) and significance of paths was tested by *t*-test. Normalization of behavioral scores and SEM were performed using the *bestNormalize* and *lavaan* packages in R, respectively.

In vivo electrophysiological recordings and histological analysis

Five male WT C57BL/6J mice (16–20 weeks old, SLC Shizuoka, Japan) with preoperative weights of 20–30 g as well as four male *Vmat1*$^{Ile/Ile}$ mice (16–20 weeks old) and four male *Vmat1*$^{Thr/Thr}$ mice (20–24 weeks old) obtained from the 2nd batch were implanted with intracranial electrodes for *in vivo* electrophysiological recordings. The animals were housed under a 12 h/12 h light/dark schedule with lights on at 7:00 AM prior to surgery. For local field potential (LFP) recordings, an array of 3 immobile tetrodes was stereotaxically implanted above the dmPFC (2.00 mm anterior and 0.50 mm lateral to bregma) at a depth of 1.40 mm and an array of 4 tetrodes was implanted in the amygdala (0.80 mm posterior and 3.00 mm lateral to bregma) at a depth of 4.40

mm using guide cannulae. Following surgery, each animal was housed in a separate transparent Plexiglas cage with free access to water and food for at least 7 days before recordings.

The mouse was connected to the recording equipment via a digitally programmable amplifier (Cereplex M, Blackrock Microsystems, Salt Lake City, UT) placed close to the animal's head. Electrical signals during elevated plus maze (see methods for detail) were sampled at 2 kHz and low-pass filtered at 500 Hz with Cereplex Direct data acquisition system. The animal's moment-to-moment position was tracked at 15 Hz using a video camera attached to the ceiling for 10 min. After a recording session, the mouse was overdosed with isoflurane, perfused intracardially with 4% paraformaldehyde (PFA) in phosphate-buffered saline (PBS, pH 7.4), and decapitated. The dissected brain was fixed overnight in 4% PFA/PBS and then cryoprotected by successive overnight incubations in 20% sucrose and 30% sucrose in PBS. Frozen coronal sections (100 µm) were cut using a microtome, mounted, and processed for cresyl violet staining. The positions of all electrodes were confirmed by identifying the corresponding electrode tracks in histological tissue sections.

RNA-sequencing and transcriptome analysis

We obtained RNA-sequencing (RNA-seq) data from 3 tissues in the brain, prefrontal cortex, amygdala, and striatum of four mice per genotype, with DNBSEQ platform at the Beijing Genomics Institute (BGI, Hong Kong, China). The raw reads were quality checked, trimmed, and filtered using fastp 0.20.0 (71), yielding 20–21 million filtered

reads per sample (Supplementary Table S4). STAR v2.7.5c (72) was then used for mapping the reads to the reference mouse genome (GRCm38.p6). We assigned reads to the Ensembl100 annotation and generated fragment counts by featureCounts (73), and the fragment counts were used to perform differential expression analysis with iDEP v0.91 workflow (74). After normalizing all counts according to effective library size, we retained genes with > 1 count per million (CPM) in half of the samples (24 samples). A total of 13,608 genes were then assessed in downstream analyses. Principal component analysis (PCA) was first performed to reveal the overall expression pattern of each sample. While most samples demonstrated distinct expression patterns, one supposed amygdala sample (derived from a 4-month-old *Vmat1*$^{Thr/Thr}$ mouse) exhibited an expression pattern similar to the other striatal samples (Supplementary Fig. S20). Given the inconsistency in the expression pattern, we excluded this sample and conducted the normalization step again for the remaining 47 samples.

We conducted pair-wise between-genotype comparisons of the same brain regions to identify differentially expressed genes (DEGs), which were defined by |log2(fold change)| > 1 and false discovery rate (FDR; corrected by the Benjamini and Hochberg method) < 0.05. The DEGs were further characterized by enrichment analysis for gene ontology (GO) terms in the iDEP pipeline. An Illumina BaseSpace application (http://basespace.illumina.com/apps) was used to investigate the correlation in expression levels of DEGs among currently and previously collected datasets. To identify specific biological pathways affected by *Vmat1* genotypes, we conducted weighted gene correlation network analysis (WGCNA) (75) of 15 samples from the

amygdala. The 1000 genes with most variable expression levels (largest coefficients of variation) among samples were retained, and the correlations among gene expression levels across samples were then calculated to detect co-expressing modules. We also calculated the correlations between the expression levels of a given gene in the amygdala and the behavioral composite (locomotor activity and anxiety), based on the data collected from 8 individuals (two for each genotype). Genes belonging to modules of interest were further included in protein-protein interaction networks constructed using STRING, and functional gene clusters were detected by the MCODE module of Cytoscape 3.8.2 (76).

Acknowledgments

Some of the computations for transcriptomic analyses were performed on the NIG supercomputer at ROIS National Institute of Genetics. We thank Dr. Liu Jinsha and Ms. Eriko Koike for technical assistance with mouse embryo manipulations and care of newborns, Ms. Chikako Ozeki and Tamaki Murakami for their assistance with behavioral experiments, and Drs. Masayuki Koganezawa and Noriko Osumi for their valuable comments on the manuscript. This work was supported by the Japan Society for the Promotion of Science (Grants-in-Aid for Scientific Research 17H05934, 19H04892, and 16H06276 (AdAMS) to MK, 20J12055 to DXS, 17H05939 and 19H04897 to TS, 17H05967 and 19H04922 to YUI, and 16H06276 to TM) and Intramural Research Grants for Neurological and Psychiatric Disorder of NCNP (27-7, 30-9, and 3-9 to TI). This work was also supported by MEXT Promotion of Distinctive Joint Research Center Program (Grant Number JPMXP0618217663).

Author contributions

DXS and MK conceived and DXS, YUI, SH, TK, and TS designed the study. DXS, YUI, TI, TM, TS, and MK acquired funding. YUI and YM conducted genome-editing experiments with mice. DXS, SH, KN, and TK designed and DXS and SH performed behavioral tests. DXS analyzed behavioral test results with the help of SH and GS. NK and TS performed electrophysiological and histological experiments. TS dissected all the brain samples for RNA-Seq, for which DXS and HH performed data analysis. DXS,

565 YUI, TI, SH, TS, and MK wrote the manuscript with contributions and revisions from

566 all authors. All authors have read and approved the final manuscript.

567

568 **Competing interest statement**

569 The authors declare no competing interests.

References

1. A. M. M. Sousa, K. A. Meyer, G. Santpere, F. O. Gulden, N. Sestan, Evolution of the human nervous system function, structure, and development. *Cell* **170**, 226–247 (2017).

2. M. A. Raghanti, *et al.*, A neurochemical hypothesis for the origin of hominids. *Proc. Natl. Acad. Sci. U. S. A.* **115**, E1108–E1116 (2018).

3. Y. Zhu, *et al.*, Spatiotemporal transcriptomic divergence across human and macaque brain development. *Science* **362**, eaat8077 (2018).

4. R. Pryluk, Y. Kfir, H. Gelbard-Sagiv, I. Fried, R. Paz, A tradeoff in the neural code across regions and species. *Cell* **176**, 1–13 (2019).

5. R. Cools, A. C. Roberts, T. W. Robbins, Serotoninergic regulation of emotional and behavioural control processes. *Trends Cogn. Sci.* **12**, 31–40 (2008).

6. D. Shohamy, R. A. Adcock, Dopamine and adaptive memory. *Trends Cogn. Sci.* **14**, 464–472 (2010).

7. R. P. Ebstein, S. Israel, S. H. Chew, S. Zhong, A. Knafo, Genetics of human social behavior. *Neuron* **65**, 831–844 (2010).

8. A. M. M. Sousa, Y. Zhu, M. A. Raghanti, R. R. Kitchen, M. Onorati, Molecular and cellular reorganization of neural circuits in the human lineage. *Science* **358**, 1027–1032 (2017).

9. C. M. Bergey, J. E. Phillips-Conroy, T. R. Disotell, C. J. Jolly, Dopamine pathway is highly diverged in primate species that differ markedly in social behavior. *Proc. Natl. Acad. Sci. U. S. A.* **113**, 6178–6181 (2016).

592 10. N. Staes, *et al.*, Serotonin receptor 1A variation is associated with anxiety and
593 agonistic behavior in chimpanzees. *Mol. Biol. Evol.* **36**, 1418–1429 (2019).
594 11. D. X. Sato, M. Kawata, Positive and balancing selection on SLC18A1 gene
595 associated with psychiatric disorders and human-unique personality traits. *Evol.*
596 *Lett.* **2**, 499–510 (2018).
597 12. J. D. Erickson, M. K.-H. Schäfer, T. I. Bonner, L. E. Eiden, E. Weihe, Distinct
598 pharmacological properties and distribution in neurons and endocrine cells of two
599 isoforms of the human vesicular monoamine transporter. *Proc. Natl. Acad. Sci.*
600 *U. S. A.* **93**, 5166–5171 (1996).
601 13. K. M. Lohr, *et al.*, Increased vesicular monoamine transporter enhances
602 dopamine release and opposes Parkinson disease-related neurodegeneration in
603 vivo. *Proc. Natl. Acad. Sci. U. S. A.* **111**, 9977–82 (2014).
604 14. F. W. Lohoff, *et al.*, Functional genetic variants in the vesicular monoamine
605 transporter 1 modulate emotion processing. *Mol. Psychiatry* **19**, 129–139 (2014).
606 15. D. X. Sato, Y. Ishii, T. Nagai, K. Ohashi, M. Kawata, Human-specific mutations
607 in VMAT1 confer functional changes and multi-directional evolution in the
608 regulation of monoamine circuits. *BMC Evol. Biol.* **19**, 220 (2019).
609 16. F. W. Lohoff, *et al.*, Variations in the vesicular monoamine transporter 1 gene
610 (VMAT1/SLC18A1) are associated with bipolar I disorder.
611 *Neuropsychopharmacology* **31**, 2739–2747 (2006).
612 17. F. W. Lohoff, *et al.*, Association between variation in the vesicular monoamine
613 transporter 1 gene on chromosome 8p and anxiety-related personality traits.

Neurosci. Lett. **434**, 41–45 (2008).

18. M. Vaht, E. Kiive, T. Veidebaum, J. Harro, A functional vesicular monoamine transporter 1 (VMAT1) gene variant is associated with affect and the prevalence of anxiety, affective, and alcohol use disorders in a longitudinal population-representative birth cohort study. *Int. J. Neuropsychopharmacol.* **19**, 1–9 (2016).

19. A. Adhikari, M. A. Topiwala, J. A. Gordon, Synchronized Activity between the Ventral Hippocampus and the Medial Prefrontal Cortex during Anxiety. *Neuron* **65**, 257–269 (2010).

20. E. Likhtik, J. M. Stujenske, M. A. Topiwala, A. Z. Harris, J. A. Gordon, Prefrontal entrainment of amygdala activity signals safety in learned fear and innate anxiety. *Nat. Neurosci.* **17**, 106–113 (2014).

21. O. Bukalo, *et al.*, Prefrontal inputs to the amygdala instruct fear extinction memory formation. *Sci. Adv.* **1**, 1–9 (2015).

22. P. L. A. Gabbott, T. A. Warner, P. R. L. Jays, P. Salway, S. J. Busby, Prefrontal cortex in the rat: Projections to subcortical autonomic, motor, and limbic centers. *J. Comp. Neurol.* **492**, 145–177 (2005).

23. D. Peter, *et al.*, Differential expression of two vesicular monoamine transporters. *J. Neurosci.* **15**, 6179–6188 (1995).

24. B. Schütz, M. K. H. Schäfer, L. E. Eiden, E. Weihe, Vesicular amine transporter expression and isoform selection in developing brain, peripheral nervous system and gut. *Dev. Brain Res.* **106**, 181–204 (1998).

25. R. Noroozi, *et al.*, Association study of the vesicular monoamine transporter 1

(VMAT1) gene with autism in an Iranian population. *Gene* **625**, 10–14 (2017).

26. A. C. Need, *et al.*, Pharmacogenetics of antipsychotic response in the CATIE trial: a candidate gene analysis. *Eur. J. Hum. Genet.* **17**, 946–957 (2009).

27. M. Davis, D. L. Walker, L. Miles, C. Grillon, Phasic vs sustained fear in rats and humans: Role of the extended amygdala in fear vs anxiety. *Neuropsychopharmacology* **35**, 105–135 (2010).

28. P. Tovote, J. P. Fadok, A. Lüthi, Neuronal circuits for fear and anxiety. *Nat. Rev. Neurosci.* **16**, 317–331 (2015).

29. B. Kim, *et al.*, Dopamine D2 receptor-mediated circuit from the central amygdala to the bed nucleus of the stria terminalis regulates impulsive behavior. *Proc. Natl. Acad. Sci. U. S. A.* **115**, E10730–E10739 (2018).

30. L. J. Matthews, P. M. Butler, Novelty-seeking DRD4 polymorphisms are associated with human migration distance Out-of-Africa after controlling for neutral population gene structure. **145**, 382–389 (2011).

31. J. Y. Chen, E. A. Wang, C. Cepeda, M. S. Levine, Dopamine imbalance in Huntington's disease: A mechanism for the lack of behavioral flexibility. *Front. Neurosci.* **7**, 1–14 (2013).

32. F. W. Lohoff, G. V. Carr, B. Brookshire, T. N. Ferraro, I. Lucki, Deletion of the vesicular monoamine transporter 1 (vmat1/slc18a1) gene affects dopamine signaling. *Brain Res.* **1712**, 151–157 (2019).

33. W. Enard, *et al.*, Molecular evolution of FOXP2, a gene involved in speech and language. *Nature* **418**, 869–872 (2002).

658 34. W. Enard, *et al.*, A humanized version of Foxp2 affects cortico-basal ganglia
659 circuits in mice. *Cell* **137**, 961–971 (2009).
660 35. E. Spiteri, *et al.*, Identification of the transcriptional targets of FOXP2, a gene
661 linked to speech and language, in developing human brain. *Am. J. Hum. Genet.*
662 **81**, 1144–1157 (2007).
663 36. S. C. Vernes, *et al.*, Foxp2 regulates gene networks implicated in neurite
664 outgrowth in the developing brain. *PLoS Genet.* **7**, e1002145 (2011).
665 37. B. Wang, T. Lufkin, J. L. R. Rubenstein, Dlx6 regulates molecular properties of
666 the striatum and central nucleus of the amygdala. *J. Comp. Neurol.* **519**, 2320–
667 2334 (2011).
668 38. L. A. Ehrman, *et al.*, The LIM homeobox gene Isl1 is required for the correct
669 development of the striatonigral pathway in the mouse. *Proc. Natl. Acad. Sci. U.*
670 *S. A.* **110**, E4027 (2013).
671 39. Z. Xu, *et al.*, SP8 and SP9 coordinately promote D2-type medium spiny neuron
672 production by activating Six3 expression. *Development* **145** (2018).
673 40. K. M. Sousa, *et al.*, Wnt2 regulates progenitor proliferation in the developing
674 ventral midbrain. *J. Biol. Chem.* **285**, 7246–7253 (2010).
675 41. P. K. Multani, *et al.*, VMAT1 deletion causes neuronal loss in the hippocampus
676 and neurocognitive deficits in spatial discrimination. *Neuroscience* **232**, 32–44
677 (2013).
678 42. J. M. Revest, *et al.*, Adult hippocampal neurogenesis is involved in anxiety-
679 related behaviors. *Mol. Psychiatry* **14**, 959–967 (2009).

680 43. C. Anacker, R. Hen, Adult hippocampal neurogenesis and cognitive flexibility-
681 linking memory and mood. *Nat. Rev. Neurosci.* **18**, 335–346 (2017).
682 44. K. M. Tye, *et al.*, Amygdala circuitry mediating reversible and bidirectional
683 control of anxiety. *Nature* **471**, 358–362 (2011).
684 45. P. H. Janak, K. M. Tye, From circuits to behaviour in the amygdala. *Nature* **517**,
685 284–292 (2015).
686 46. M. P. de la Mora, A. Gallegos-Cari, Y. Arizmendi-García, D. Marcellino, K.
687 Fuxe, Role of dopamine receptor mechanisms in the amygdaloid modulation of
688 fear and anxiety: Structural and functional analysis. *Prog. Neurobiol.* **90**, 198–
689 216 (2010).
690 47. S. R. Hansson, B. J. Hoffman, É. Mezey, Ontogeny of vesicular monoamine
691 transporter mRNAs VMAT1 and VMAT2. I. The developing rat central nervous
692 system. *Dev. Brain Res.* **110**, 135–158 (1998).
693 48. E. A. Murray, The amygdala, reward and emotion. *Trends Cogn. Sci.* **11**, 489–
694 497 (2007).
695 49. J. Posner, *et al.*, Alterations in amygdala-prefrontal circuits in infants exposed to
696 prenatal maternal depression. *Transl. Psychiatry* **6**, e935 (2016).
697 50. X. Chang, *et al.*, RNA-seq analysis of amygdala tissue reveals characteristic
698 expression profiles in schizophrenia. *Transl. Psychiatry* **7**, e1203 (2017).
699 51. T. A. Avino, *et al.*, Neuron numbers increase in the human amygdala from birth
700 to adulthood, but not in autism. *Proc. Natl. Acad. Sci. U. S. A.* **115**, 3710–3715
701 (2018).

52. T. Asari, *et al.*, Amygdalar enlargement associated with unique perception. *Cortex* **46**, 94–99 (2010).

53. K. Rice, B. Viscomi, T. Riggins, E. Redcay, Amygdala volume linked to individual differences in mental state inference in early childhood and adulthood. *Dev. Cogn. Neurosci.* **8**, 153–163 (2014).

54. K. C. Bickart, C. I. Wright, R. J. Dautoff, B. C. Dickerson, L. F. Barrett, Amygdala volume and social network size in humans. *Nat. Neurosci.* **14**, 163–164 (2011).

55. J. Sallet, *et al.*, Social network size affects neural circuits in macaques. *Science* **334**, 697–700 (2011).

56. S. Atzil, *et al.*, Dopamine in the medial amygdala network mediates human bonding. *Proc. Natl. Acad. Sci. U. S. A.* **114**, 2361–2366 (2017).

57. K. C. Bickart, B. C. Dickerson, L. F. Barrett, The amygdala as a hub in brain networks that support social life. *Neuropsychologia* **63**, 235–248 (2014).

58. C. Schreiweis, *et al.*, Humanized Foxp2 accelerates learning by enhancing transitions from declarative to procedural performance. *Proc. Natl. Acad. Sci. U. S. A.* **111**, 14253–14258 (2014).

59. F. Zhu, R. R. Nair, E. M. C. Fisher, T. J. Cunningham, Humanising the mouse genome piece by piece. *Nat. Commun.* **10**, 1845 (2019).

60. N. R. Wray, *et al.*, Genome-wide association analyses identify 44 risk variants and refine the genetic architecture of major depression. *Nat. Genet.* **50**, 668–681 (2018).

724 61. S. Ripke, *et al.*, Biological insights from 108 schizophrenia-associated genetic
725 loci. *Nature* **511**, 421–427 (2014).
726 62. M. T. Lo, *et al.*, Genome-wide analyses for personality traits identify six
727 genomic loci and show correlations with psychiatric disorders. *Nat. Genet.* **49**,
728 152–156 (2017).
729 63. F. W. Lohoff, *et al.*, Association between polymorphisms in the vesicular
730 monoamine transporter 1 gene (VMAT1/SLC18A1) on chromosome 8p and
731 schizophrenia. *Neuropsychobiology* **57**, 55–60 (2008).
732 64. A. Waterhouse, *et al.*, SWISS-MODEL: homology modelling of protein
733 structures and complexes. *Nucleic Acids Res.* **46**, W296–W303 (2018).
734 65. Y. Choi, A. P. Chan, PROVEAN web server: a tool to predict the functional
735 effect of amino acid substitutions and indels. *Bioinformatics* **31**, 2745–2747
736 (2015).
737 66. P. Kumar, S. Henikoff, P. C. Ng, Predicting the effects of coding non-
738 synonymous variants on protein function using the SIFT algorithm. *Nat. Protoc.*
739 **4**, 1073–1081 (2009).
740 67. C. H. M. Rodrigues, D. E. V. Pires, D. B. Ascher, DynaMut: predicting the
741 impact of mutations on protein conformation, flexibility and stability. *Nucleic*
742 *Acids Res.* **46**, W350–W355 (2018).
743 68. M. Hashimoto, Y. Yamashita, T. Takemoto, Electroporation of Cas9
744 protein/sgRNA into early pronuclear zygotes generates non-mosaic mutants in
745 the mouse. *Dev. Biol.* **418**, 1–9 (2016).

69. J. P. Concordet, M. Haeussler, CRISPOR: Intuitive guide selection for CRISPR/Cas9 genome editing experiments and screens. *Nucleic Acids Res.* **46**, W242–W245 (2018).

70. R. B. Kline, *Principles and Practice of Structural Equation Modeling*, D. A. Kenny, T. D. Little, Eds., 4th Edi. (The Guilford Press, 2016).

71. S. Chen, Y. Zhou, Y. Chen, J. Gu, fastp: an ultra-fast all-in-one FASTQ preprocessor. *Bioinformatics* **34**, i884–i890 (2018).

72. A. Dobin, *et al.*, STAR: ultrafast universal RNA-seq aligner. *Bioinformatics* **29**, 15–21 (2013).

73. Y. Liao, G. K. Smyth, W. Shi, featureCounts: an efficient general purpose program for assigning sequence reads to genomic features. *Bioinformatics* **30**, 923–930 (2014).

74. S. X. Ge, E. W. Son, R. Yao, iDEP: An integrated web application for differential expression and pathway analysis of RNA-Seq data. *BMC Bioinformatics* **19**, 1–24 (2018).

75. P. Langfelder, S. Horvath, WGCNA: An R package for weighted correlation network analysis. *BMC Bioinformatics* **9**, 559 (2008).

76. P. Shannon, *et al.*, Cytoscape: a software environment for untegrated models. *Genome Res.* **13**, 2498–2504 (2003).

Tables and Figures

Table 1. *In silico* prediction of mVMAT1 tolerance to the humanized mutations Asn133Thr and Asn133Ile. Text in bold indicates significant effects of the substitutions as predicted by Provean score < –2.5 or SIFT score < 0.05. The Provean term "Deleterious" and SIFT term "Damaging" refer to significant effects on protein function but do not necessarily indicate that they deteriorate protein function. All three methods predict that 133Ile has greater effects than 133Thr on mVMAT1 function.

Ref.	Alt.	Provean		SIFT		DynaMut	
		Score	Prediction	Score	Prediction	ΔΔG (kcal/mol)	Prediction
Asn	Thr	**-3.27**	**Deleterious**	0.243	Tolerated	-0.062	Destabilizing
Asn	Ile	**-6.55**	**Deleterious**	**0.014**	**Damaging**	1.106	Stabilizing

776 **Table 2. List of gene ontology (GO) terms significantly overrepresented in the set**

777 **of differentially expressed genes (DEGs) between *Vmat1*^{WT} and *Vmat1*$^{Ile/Ile}$ mice.**

778 *P* values were corrected by the Benjamini-Hochberg method. Only terms with $P < 0.05$

779 are presented. Downregulation indicates *Vmat1*^{WT} > *Vmat1*$^{Ile/Ile}$ while upregulation

780 indicates *Vmat1*$^{Ile/Ile}$ > *Vmat1*^{WT}.

Direction	Pathways	Genes	adj.Pval
Upregulated	Regulation of cell junction assembly	*Ace*, *Cldn1*, *Enpp2*	5.5×10^{-3}
Downregulated	Locomotory behavior	*Gng7*, *Gpr88*, *Ido1*, *Pde1b*, *Penk*, *Ppp1r1b*, *Rasd2*	7.2×10^{-5}
Downregulated	Behavior	*Asic4*, *Foxp1*, *Gng7*, *Gpr88*, *Ido1*, *Pde1b*, *Penk*, *Ppp1r1b*, *Rasd2*	4.9×10^{-4}
Downregulated	Mononuclear cell differentiation	*Cd4*, *Foxp1*, *Pde1b*	2.8×10^{-3}
Downregulated	Response to amphetamine	*Pde1b*, *Ppp1r1b*, *Rgs9*	2.8×10^{-3}
Downregulated	Multicellular organismal response to stress	*Asic4*, *Gng7*, *Ido1*, *Penk*	2.8×10^{-3}
Downregulated	Cardiac muscle tissue development	*Foxp1*, *Myom3*, *Rarb*, *Rbp4*, *Wnt2*	3.9×10^{-3}
Downregulated	Regulation of cardiac muscle cell proliferation	*Foxp1*, *Rbp4*, *Wnt2*	4.0×10^{-3}
Downregulated	Behavioral fear response	*Asic4*, *Gng7*, *Penk*	4.6×10^{-3}
Downregulated	cAMP catabolic process	*Pde7b*, *Pde10a*	4.8×10^{-3}

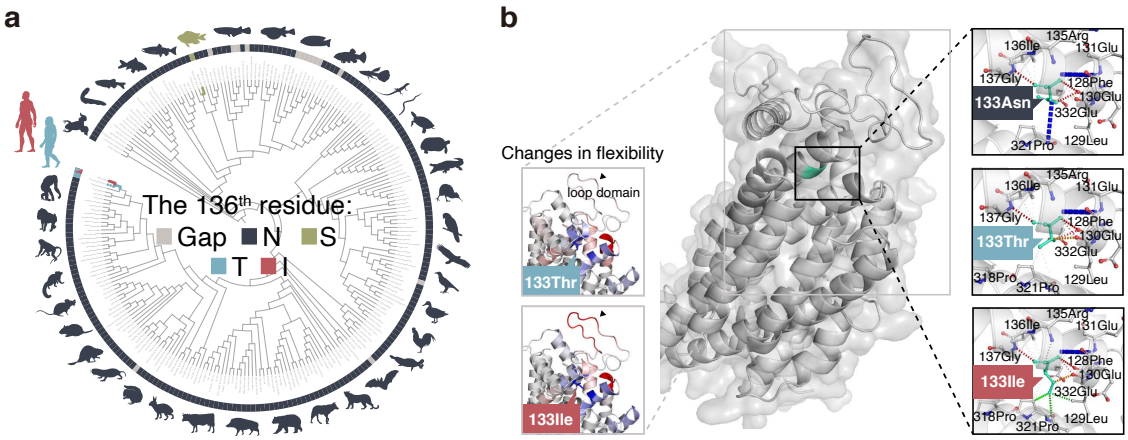

Figure 1. An ultra-conserved residue in VMAT1 exhibits functional variants unique to humans. (a) A phylogenetic tree constructed by multiple sequence alignment of the *VMAT1* gene. Almost all genes across 236 vertebrate species retain asparagine (N, Asn) on the 136th residue, while humans are the only vertebrate species except for bicolor damselfish (shown in green) with a unique polymorphism (T/I, Thr136Ile; rs1390938). Note that the phylogenetic relationship presented here is not necessarily consistent with the known species tree. **(b)** mVMAT1 protein structure predicted by homology modeling and the effects of human-type mutagenesis (corresponding to 133Thr and 133Ile in mVMAT1). (Left) Δ Vibrational entropy energy between WT (133Asn) and mutants. Amino acids are colored according to the vibrational entropy change conferred by the given mutation. Red represents a gain of flexibility and blue represents a rigidification of the structure. The 133Ile mutation leads to increased flexibility of the first luminal loop, a receptor-like domain affecting the affinity of ligands. (Right) When introduced *in silico*, 133Ile but not 13Thr exhibits hydrophobic interactions (shown by green dotted line) with surrounding sites, which likely influence the folding and/or stability of mVMAT1 protein. Blue, red, and orange dotted lines

798 represent amide bonds, hydrogen bonds, and weak van der Waals interactions,

799 respectively.

800

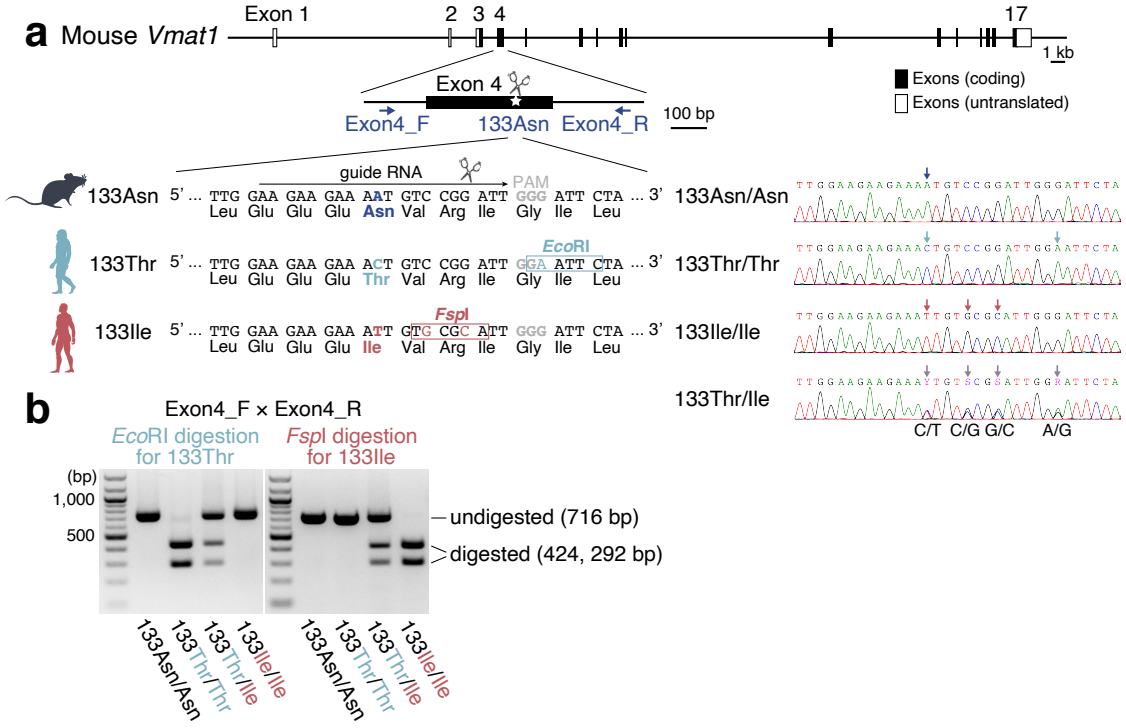

Figure 2. Generation of the *Vmat1*-humanized mouse models by CRISPR/Cas9 genome editing. (a) Targeting strategy for mVMAT1 133Asn humanization. Genetic configuration of the mouse *Vmat1* gene is shown above. Exon 4 encoding 133Asn is enlarged, and the primers used for genotyping (Exon4_F and Exon4_R) are depicted. To replace the mouse 133Asn with 133Thr or 133Ile by CRISPR/Cas9-mediated genome engineering, a guide RNA with minimum off-target effects was designed. GGG (gray) represents the PAM sequence. In addition to 133Asn humanization, restriction enzyme recognition sites (*Eco*RI and *Fsp*I) were synonymously incorporated to avoid the unwanted re-editing and to simplify genotyping. Sanger sequencing profiles of 133Asn/Asn (WT), 133Thr/Thr, 133Ile/Ile, and 133Thr/Ile are shown on the right. **(b)** PCR-RFLP assay, in which PCR products amplified using Exon4_F and Exon4_R were

813 digested by *Eco*RI and *Fsp*I, respectively, could be used to distinguish 4 genotypes

814 without sequencing.

815

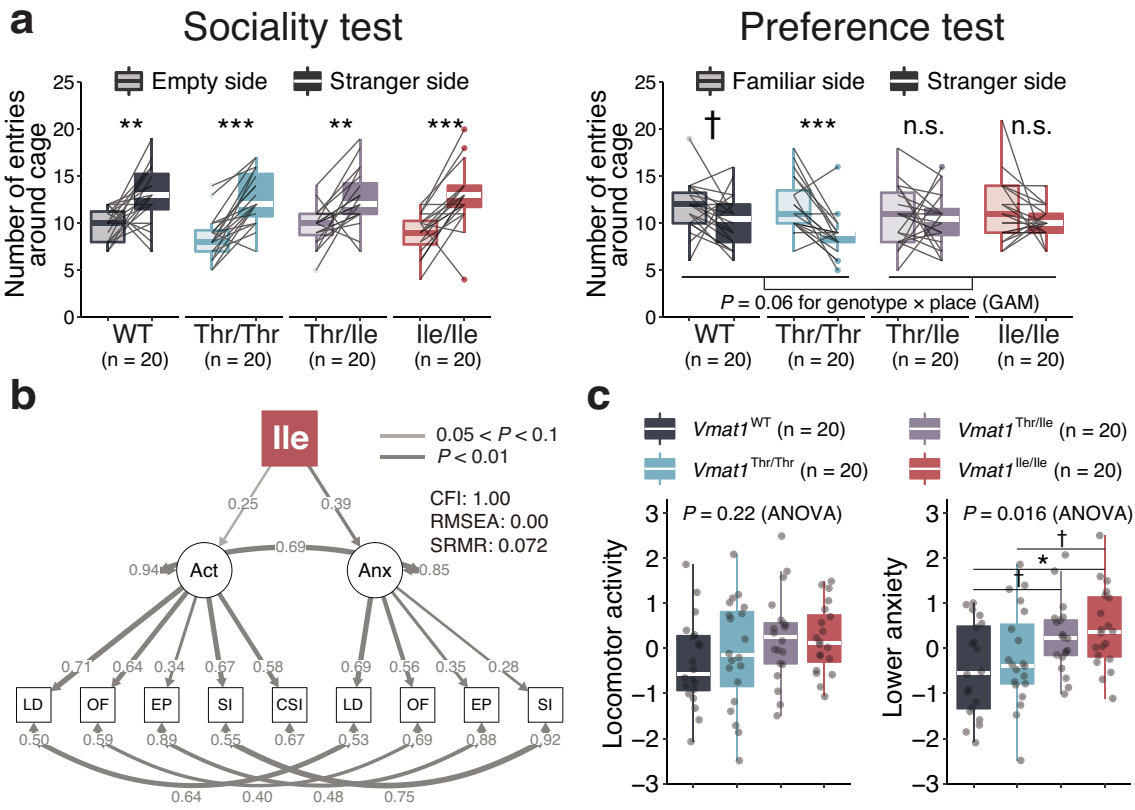

Figure 3. Comprehensive behavioral tests reveal distinct behavioral changes in *Vmat1*$^{Thr/Thr}$ and *Vmat1*^{Ile} mice, including reduced anxiety. (a) In Crawley's social interaction test, *Vmat1*$^{Thr/Thr}$ mice preferred a familiar (previously exposed) mouse over a novel stranger. **(b)** Structural Equation Modeling (SEM) revealed the best fit model to explain the effects of *Vmat1* genotype on locomotor activity (Act) and anxiety (Anx). According to the model, *Vmat1*^{Ile} (*Vmat1*$^{Thr/Ile}$ and *Vmat1*$^{Ile/Ile}$) significantly reduces anxiety-like behavior. The boxes and circles represent measured and latent variables, respectively. The paths represent causal relationships on which numerical values indicate standardized coefficient and the gray-scale intensity of the paths indicates statistical significance tested by *t*-test. See Methods for the detailed modeling procedure. **(c)** *Vmat1*^{Ile} mice exhibited lower anxiety than WT and *Vmat1*$^{Thr/Thr}$

828 genotypes. See Methods for the detailed calculation of the scores. For the composite
829 anxiety score, a higher value indicates lower anxiety. Statistical significance was
830 evaluated by paired *t*-test for **(a),** and by pair-wise *t*-test with FDR correction by the
831 Benjamini-Hochberg method for **(c)**. Interactive effects of genotype (Ile allele labeled
832 by 1, and 0 otherwise) and cage place were also assessed by generalized additive model
833 with quasi-Poisson distribution in **(a)**. †: $0.05 < P < 0.1$, *: $0.01 < P < 0.05$, **: $0.001 <$
834 $P < 0.01$, ***: $P < 0.001$.
835

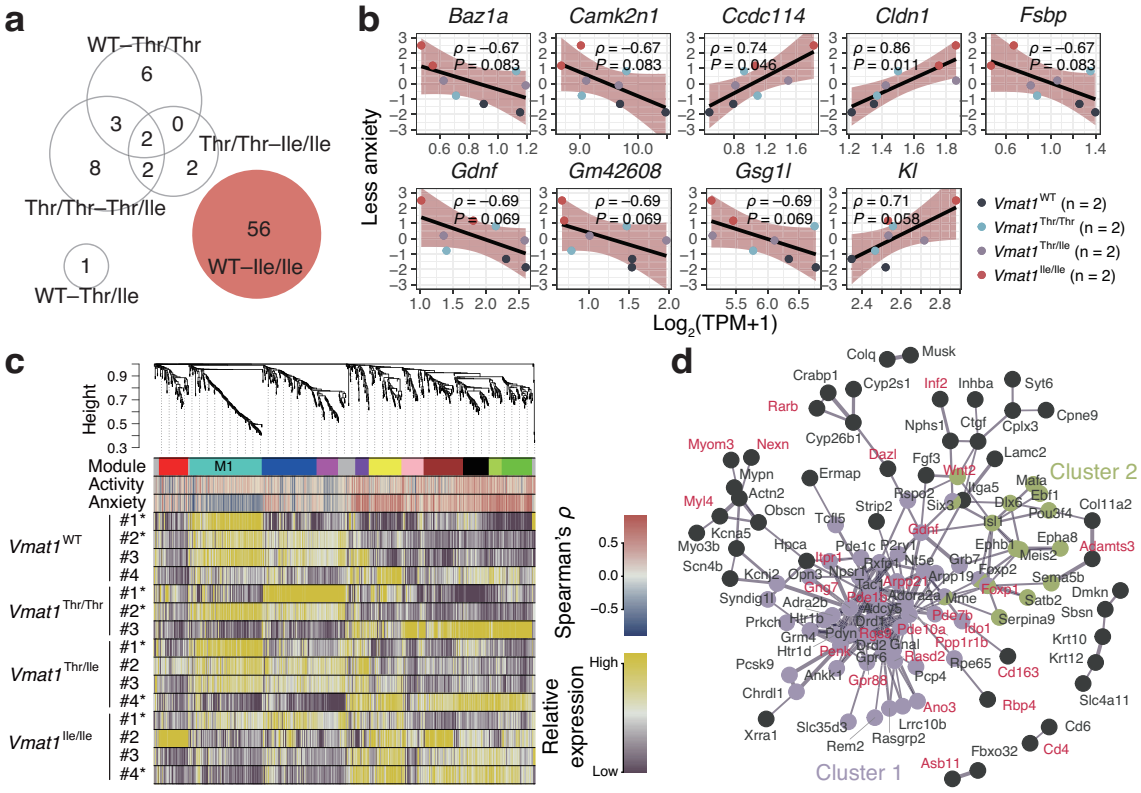

836

837 **Figure 4. Differentially expressed genes (DEGs) in the brain among *Vmat1***

838 **genotypes and predicted co-expressing modules**. **(a)** The number of DEGs detected

839 by pair-wise comparisons among the four genotypes. All DEGs were found in the

840 amygdala (with none in prefrontal cortex or striatum). **(b)** Correlations between

841 individual DEG expression levels for the WT vs. and *Vmat1*$^{Ile/Ile}$ comparison and

842 composite anxiety scores from LD, EP, OF, and SI tests (see Methods). Only genes with

843 strong Spearman's correlations ($P < 0.1$) are shown. The bands are 95% confidence

844 intervals. **(c)** Network dendrogram from co-expression modules based on the expression

845 data of all 47 regional brain samples. Each branch represents an individual gene, and the

846 colors below represent the module, correlation (ρ) with behavioral phenotype

847 (locomotor activity and anxiety), and the relative expression level in the amygdala

848 across genotypes. The samples with asterisks are from mice with behavioral data and

849 were used to calculate the correlations between expression levels and behavioral
850 phenotypes. The M1 module (shown in turquoise), showing negative correlations with
851 anxiety score exhibited significant overrepresentation of the DEGs detected between
852 WT and *Vmat1*$^{Ile/Ile}$ mice. **(d)** Protein–protein interaction networks among the genes in
853 M1. The DEGs detected between WT and *Vmat1*$^{Ile/Ile}$ mice are shown in red. The
854 thickness of the line indicates the strength of data support analyzed by STRING.
855

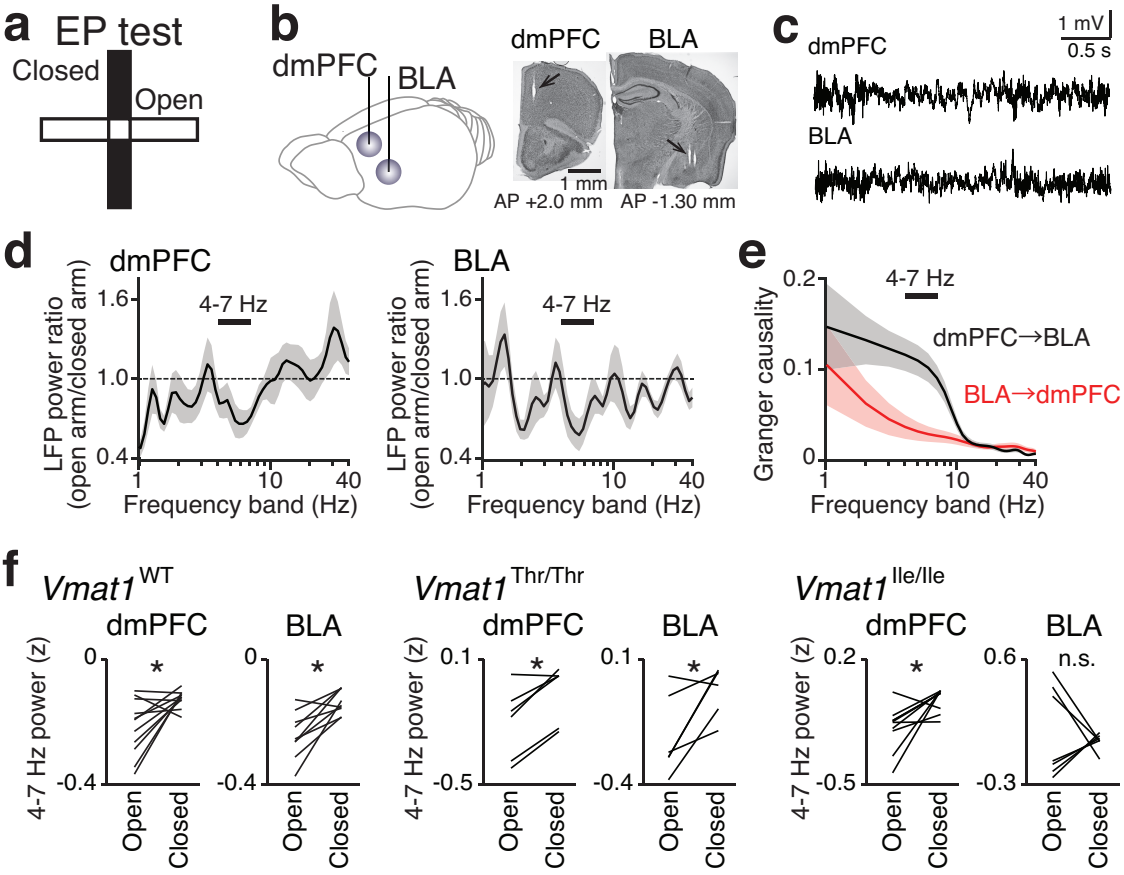

Figure 5. Wild-type and *Vmat1*$^{Thr/Thr}$ mice, but not *Vmat1*$^{Ile/Ile}$ mice, exhibit a reduction in amygdalar 4–7 Hz local field potential (LFP) power under anxiogenic conditions. (a) (Left) LFP recordings were simultaneously performed from the dorsomedial prefrontal cortex (dmPFC) and basolateral amygdala (BLA). (Right) Histological confirmation of electrode locations in the dmPFC and BLA. **(b)** Typical LFP signals from the dmPFC and BLA. **(c)** An elevated plus maze (EP) test. **(d)** Spectrograms of dmPFC (left) and BLA (right) LFP power in (anxiogenic) open arms relative to closed arms. Data were averaged from all *Vmat1*^{WT} mice. The bar above indicates the 4–7 Hz band, showing pronounced decreases in LFP power in both regions. **(e)** Spectral Granger causality averaged over 20 dmPFC–BLA electrode pairs.

867 **(f)** Comparison of dmPFC and BLA LFP 4–7 Hz power (z-scored) between open and

868 closed arms. *$P < 0.05$, paired *t*-test. Each line represents one electrode.

869

870